Rates and Products of the Dissociative Recombination of $C_3H_7^+$ in Low-Energy Electron Collisions

Anneli Ehlerding,*,† Susan T. Arnold,‡ A. A. Viggiano,‡ Shirzad Kalhori,† Jacek Semaniak,§ Alik M. Derkatch,† S. Rosén,† Magnus af Ugglas,|| and Mats Larsson†

Department of Physics, SCFAB, Stockholm University, SE-106 91 Stockholm, Sweden, Air Force Research Laboratory, Space Vehicles Directorate, 29 Randolph Rd, Hanscom AFB, Massachusetts 01731, Institute of Physics, Swietokrzyska Academy, 25-406 Kielce, Poland, and Manne Siegbahn Laboratory, Stockholm University, SE-104 05 Stockholm, Sweden

Received: December 16, 2002; In Final Form: January 29, 2003

This paper presents a study of the dissociative recombination of $C_3H_7^+$ with electrons in a heavy-ion storage ring, CRYRING. Cross sections were measured as a function of kinetic energy and found to be extremely rapid with a dependence of $E^{-1.10\pm0.01}$. The recombination cross section was integrated to yield a thermal rate coefficient of 1.9×10^{-6} cm^3 s^{-1}. Product branching ratios were measured and proved to be quite complex. Although 16 channels are energetically accessible at 0 eV, it was not possible to assign branching ratios to all channels; some related channels were combined in the analysis. The results show that the dissociation channel corresponding to loss of a single hydrogen atom dominates, with a branching ratio of 0.42. Multiple H-loss channels are also observed. Product channels that involve breaking a C−C bond have a combined branching ratio ranging from 0.34 to 0.39.

Introduction

Plasma-based technologies have been proposed for application in high-speed aerospace vehicles. One such application involves the use of plasmas to enhance combustion in air breathing scramjet engines. Kinetic modeling has demonstrated that introducing plasma species (positive ions and electrons) into a simple combustor can significantly reduce the ignition delay time and thus enhance reactor efficiency.[1]

The predicted improvements in combustion efficiency are due to several factors. Consider, for example, the ion kinetic mechanism for the air plasma ion, NO^+, reacting with an aliphatic fuel, octane, which involves the following steps:

$$NO^+ + C_8H_{18} \rightarrow C_8H_{17}^+ + HNO \text{ (initiation)}$$

$$C_8H_{17}^+ \rightarrow C_4H_9^+, C_3H_7^+, \text{ etc (decomposition)}$$

$$C_3H_7^+ + C_8H_{18} \rightarrow C_8H_{17}^+ + C_3H_8 \text{ (secondary reactions)}$$

$$C_3H_7^+ + e^- \rightarrow \text{neutral products (termination)}$$

Many reactions of air plasma ions with fuel components have been studied, sometimes at temperatures as high as 1400 K.[2] From this work, it is known that ions, although present in small abundance, react much more rapidly with the fuel components than do neutral reagents. The initiation reactions generally occur via hydride transfer (as shown above), proton transfer, or charge transfer, proceeding at or near the collision rate. The large ionized fuel molecules thermally decompose at combustion temperatures, yielding smaller fragment ions, principally $C_4H_9^+$, $C_3H_7^+$, and $C_2H_5^+$. These small hydrocarbon ions undergo secondary hydride transfer reactions with the fuel in a cycle that regenerates large ionized fuels. Together, the initiation, decomposition, and secondary reactions enhance combustion efficiency by increasing the overall heat release in the system and by breaking down the large fuel molecules. However, the most significant contribution to the enhanced efficiency comes from the production of radical species, which serve as chain initiators and combustion propagators. Production of radicals occurs not only through the ion−molecule reactions but also from the plasma termination step, namely, the dissociative recombination (DR) of free electrons with ionized fuel fragments.

For most triatomic and larger systems, the rate constants for recombination are found to be large ($>10^{-7}$ cm^3 s^{-1}).[3,4] Rates for some hydrocarbon ions have been measured by the flowing afterglow Langmuir probe (FALP) method and are of this magnitude.[5] Until recently, however, there has been little known about the product distributions that result from recombination. The ability to study DR reactions in more detail has improved considerably with the advent of storage rings[6−8] where both rate constants as a function of energy and product distributions can be measured. Initial product distribution measurements for DR of small molecular ions have shown some surprising results.[9] In particular, dissociation channels that yield three neutral products were found to be more prevalent than had been expected.[10,11] If this is a general trend in DR reactions, it will have a significant impact on the models of plasma enhanced combustion, which to date have assumed only loss of a single hydrogen atom upon recombination.

We have recently begun a systematic study of hydrocarbon ion DR at the CRYRING heavy ion storage ring and have thus far reported on measurements of molecular ions consisting of

* To whom correspondence should be addressed. E-mail: anneli@physto.se.
† Department of Physics, SCFAB, Stockholm University.
‡ Air Force Research Laboratory.
§ Swietokrzyska Academy.
|| Manne Siegbahn Laboratory, Stockholm University.

10.1021/jp027729+ CCC: $25.00
Published on Web 03/11/2003

two carbon atoms.[12,13] Here we report DR cross sections as a function of energy from 1 meV to 1 eV and product distributions at 0 eV relative collision energy for $C_3H_7^+$. This is one of the most significant fragment ions produced by reactions of air plasma ions with aliphatic fuels. Allowing for a maximum of three dissociation products, as the earlier experiments suggest, there are 16 different dissociation channels that are energetically possible at 0 eV center-of-mass collision energy:

$$C_3H_7^+ + e \rightarrow \begin{cases} C_3H_6 + H + 5.9\ \text{eV} & \text{(a)} \\ C_3H_5 + H_2 + 6.6\ \text{eV} & \text{(b)} \\ C_3H_5 + H + H + 2.1\ \text{eV} & \text{(c)} \\ C_3H_4 + H_2 + H + 4.2\ \text{eV} & \text{(d)} \\ C_3H_3 + H_2 + H_2 + 4.9\ \text{eV} & \text{(e)} \\ C_2H_6 + CH + 3.1\ \text{eV} & \text{(f)} \\ C_2H_5 + CH_2 + 3.2\ \text{eV} & \text{(g)} \\ C_2H_4 + CH_3 + 6.3\ \text{eV} & \text{(h)} \\ C_2H_4 + CH_2 + H + 1.6\ \text{eV} & \text{(i)} \\ C_2H_4 + CH + H_2 + 1.7\ \text{eV} & \text{(j)} \\ C_2H_3 + CH_4 + 6.1\ \text{eV} & \text{(k)} \\ C_2H_3 + CH_3 + H + 1.5\ \text{eV} & \text{(l)} \\ C_2H_3 + CH_2 + H_2 + 1.3\ \text{eV} & \text{(m)} \\ C_2H_2 + CH_4 + H + 4.6\ \text{eV} & \text{(n)} \\ C_2H_2 + CH_3 + H_2 + 5.1\ \text{eV} & \text{(o)} \\ C_2H + CH_4 + H_2 + 3.3\ \text{eV} & \text{(p)} \end{cases}$$

Note that the kinetic energy release indicated for each channel assumes that products are formed in their ground state, which may not be a good assumption considering the amount of available energy.

Experimental Section

The experiments were performed at the heavy-ion storage ring CRYRING at the Manne Siegbahn Laboratory in Stockholm, Sweden. The facility and the experimental procedure have been described elsewhere[14] and will only be described briefly here. The $C_3H_7^+$ ions were produced in a hot-cathode discharge ion source by pulsing a small amount of 1-bromopropane into a helium plasma. The ions were extracted from the source at a translational energy of 40 keV. After mass selection, the ions were injected into the storage ring and accelerated to 2.23 MeV, the maximum beam energy, a value that is limited by the magnetic rigidity of the storage ring.[15] The ions were stored in the ring with a half-life of 1.5 s for 7.5 s. Typical ion current in this experiment was 0.11 μA.

Although there are three potential isomers of the $C_3H_7^+$ ion (*n*-propyl, iso-propyl, and protonated cyclopropyl), it is safe to assume that the iso-propyl isomer is the only one formed in the present experiments. Theoretical studies[16] conclude that only two global minima exist on the $C_3H_7^+$ surface, corresponding to the iso-propyl and protonated cyclopropyl isomers. The protonated cyclopropyl isomer is 30 kJ mol^{-1} higher in energy than the iso-propyl structure. There is no minimum associated with the *n*-propyl structure; it lies 110.5 kJ mol^{-1} higher in energy than the most stable iso-propyl form and appears to be a transition structure involved in the interconversion of the two more stable isomers. Mass spectrometric studies indicate that the *n*-propyl cation converts to either the iso-propyl or protonated cyclopropyl ions within 10^{-10} s.[17] Rearrangement to the iso-propyl ion is favored and is found to increase with increasing internal energy content of the ion. Further studies demonstrate that isomerization of the protonated cyclopropyl structure to the lowest energy iso-propyl structure requires $10^{-7}-10^{-5}$ seconds.[18,19] Previous measurements made in the selected ion flow tube at the Air Force Research Laboratory have demonstrated that $C_3H_7^+$ produced via ionization of 1-bromopropane results exclusively in the formation of iso-$C_3H_7^+$.[20]

In one of the twelve straight sections of the storage ring, the circulating ions are merged with a monoenergetic collinear electron beam over a length of 0.85 m. The electrons are magnetically confined to a diameter of 4 cm, and in the present experiment, the electron current was 0.315 mA. The electron velocity distribution can be described by an anisotropic Maxwell−Boltzmann distribution,[21] with a transversal temperature ($kT_\perp$) of about 2 meV and a longitudinal temperature ($kT_\parallel$) of about 0.1 meV.[22] By using electrons with the same average velocity as the ions, the random thermal motion of the ions is reduced and phase-space cooling is achieved. For a heavy ion such as $C_3H_7^+$, phase-space cooling is slow, and it is difficult to quantify the degree of cooling. The storage time of a few seconds allows for radiative cooling to 300 K internal temperature.

The electron beam also serves as a high-density electron target in electron−ion recombination experiments. After the cooling phase, which lasted 2.8 s after injection and acceleration in the present experiment, the electron velocity was detuned to the required collision energy. This energy, in the center-of-mass frame, is given by

$$\sqrt{E_{\text{cm}}} = \sqrt{E_{\text{e}}} - \sqrt{E_{\text{cool}}} \qquad (1)$$

where E_{e} is the average energy of the electrons during the measurement period and E_{cool} is the electron energy at which maximum cooling occurs, both given in the laboratory frame of reference.

When recombination between electrons and ions occurs within the interaction region, the neutral products formed will not follow the circular path of the ions determined by the dipole, quadrupole, and sextupole magnets but will continue along their original trajectory on the axis of the electron cooler. The neutral particles are detected on an energy-sensitive surface barrier detector placed 3.5 m from the end of the electron cooler. All neutral fragments originating from one DR event reach the detector at approximately the same time (i.e., all have essentially the same velocity), and each fragment impinges on the detector with an energy proportional to its kinetic energy and hence mass. This means that the fragments from DR events contribute to a signal at the ion beam energy independent of the dissociation channel, whereas neutrals that result from collisions between primary ions and the background gas contribute to lower energy features.

The H and H_2 products of some dissociation channels may be formed with a large amount of kinetic energy. In such a case, a fraction of the high kinetic energy products may not be detected because they may traverse a distance larger than the radius of the detector, which is 30.9 mm. This has been considered in the data evaluation of the branching fractions.

Cross Section and Thermal Rate Coefficient. The DR cross section was measured as a function of collision energy by detuning the electron cooler voltage, i.e., the electron energy, to energies corresponding up to 1 eV in the center-of-mass collision energy. The collision energy, *E*, is related to the difference between the mean ion and electron beam energy as

$$E = \frac{1}{2} m_{\text{e}} (v_i - v_e)^2 \qquad (2)$$

The electron energy was ramped during one second across the cooling energy. This is shown in Figure 1a, where the time scale refers to time after ion injection into the ring. The electron energy is changed at 5 s from 30 eV to almost 39 eV,

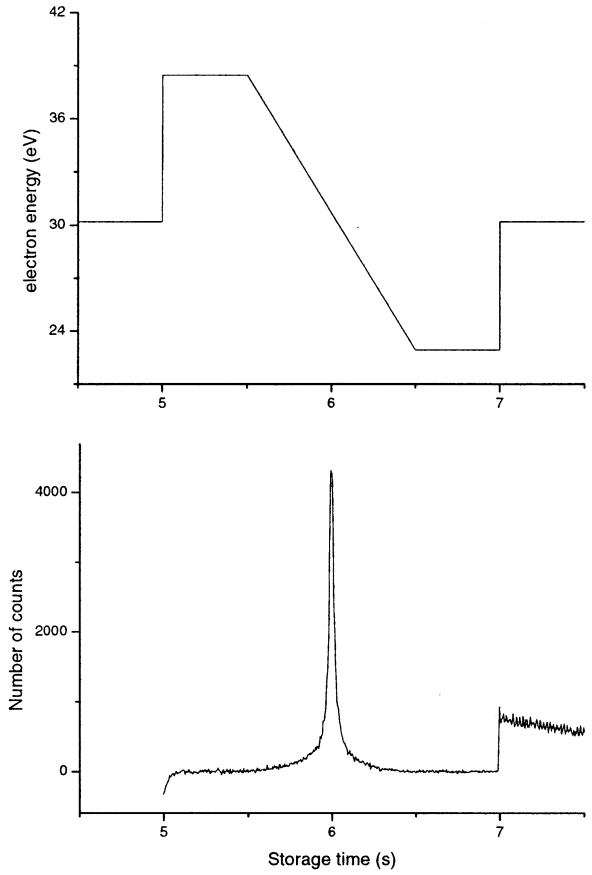

Figure 1. (a) Electron energy vs time after injection of $C_3H_7^+$. (b) Dissociative recombination total count rate on the same time scale.

corresponding to 1 eV energy difference between the ions and the electrons. The voltage is held constant for about 1 s, and then ramped to below 24 eV over 1 s. At the end of the scan cycle, the ions are ejected before a new cycle is begun.

The detector signal was monitored using a single channel analyzer in order to accept only those events corresponding to full beam energy, that is, fragments originating from a single recombination event. A multichannel scaler (MCS) recorded the number of pulses as a function of time, and this signal is shown in Figure 1b. The measurement starts 5 s after the beginning of the cycle. During the times from 5 to 5.5 s and again from 6.5 to 7 s, the signal is small corresponding to recombination at high energies. When the center-of-mass collision energy is ramped (5.5−6.5 s), a distinct symmetric peak is found. A symmetric peak is expected if the rate has a maximum at zero relative energy. This provides a convenient way to accurately determine the zero of energy including any possible contact potentials.

At collision energies significantly higher than 0 eV, the signal is considered to be only background, and thus, an exponential curve was fit to these portions and subtracted from the whole spectrum. Simultaneously, a signal from the stored ion beam was recorded on a spectrum analyzer. That signal can be related to the absolute ion current in the ring, which is measured by a current transformer at one single time.

The experimental DR rate coefficient was determined from

$$\langle v_{CM}\sigma\rangle = \frac{\nu q}{n_e l}\frac{N_{DR}}{I(t)\frac{SA1}{SA2}\Delta t} \quad (3)$$

where ν is the revolution frequency of the ions, l is the length of the interaction region (i.e., the length of the electron cooler), n_e is the electron density, N_{DR} is the number of counts coming from the DR process, and $I(t)$ is the ion current. SA1 and SA2 are two readings from the spectrum analyzer during measurement with the surface barrier detector and current transformer, respectively.

Branching Ratios. To determine branching ratios for the numerous $C_3H_7^+$ dissociative recombination channels, a grid was inserted in front of the surface barrier detectors. The grid is made of stainless steel, 50 μm thick, with holes of 70 μm diameter. The transmission of the grid has been measured in an independent experiment to be $T = 0.297 \pm 0.015$ (uncertainty at 3σ level).[23] Particles impinging on the grid can either pass through a hole in the grid or be stopped, with probabilities T and $1 - T$, respectively. Particles stopped by the grid do not contribute to the signal. Products from a DR channel resulting in two fragments can thus be detected at three different energies corresponding to the energy of each fragment and the total energy. The probability of detecting one or both of the fragments is then $T(1 - T)$ and T^2, respectively. A similar treatment can be applied to channels that produce three fragments. Note that all fragments resulting from a single recombination event travel at nearly the same velocity. Thus, an energy spectrum can be treated as a mass spectrum through $E = {}^1/_2 m v^2$.

The branching fractions were measured at 0 eV center-of-mass collision energy. It was not feasible to make measurements at higher energies because of the significantly reduced cross section. The ions were cooled at 0 eV collision energy for 2.6 s and were then held at the same energy (i.e., the electron−ion center-of-mass energy is 0 eV) during a measurement time of 4.8 s. The cooling time allowed for radiative cooling of the internal degrees of freedom.

To account for the signal contribution resulting from collisions with the residual background gas, an energy spectrum was recorded when no electron beam was present. This background spectrum was first normalized to the ion current intensity using the simultaneously recorded MCS spectrum and then subtracted from the spectrum recorded when the electron beam was present. After subtraction of the background, the energy spectrum, i.e., mass spectrum, was fit to a set of Gaussian peaks. Because the energy of the ion beam was 2.23 MeV, an absolute energy scale could be determined once the center of the peak corresponding to mass 43 was found. From the study of lighter systems where the pulse-height spectra were more resolved into separate peaks,[12,13] it is known that that Gaussian functions well describe the distributions of each fragment. The widths of the Gaussian functions were obtained by a least-squares fitting routine. The energy resolution given by this width is in agreement with the resolution in ref 13, for which the data were obtained during the same beam time week as the present data. Figure 2 shows data with the Gaussian peak fits for each mass. The areas in each of the Gaussian fits is the number of counts in each peak, i.e., for each mass; N_{3C+7H}, N_{3C+6H}, ..., N_{C+H}. As seen in the figure, the sum of the fitted peaks is essentially indistinguishable from the raw data. By considering the grid with limited transmission, these peak areas can be associated with contributions from the different dissociation channels N_a, ..., N_p through a set of linear equations. For example, the peak corresponding to the mass of C + 2H receives contributions from channel g with a probability of $T(1 - T)$ and from channel i and m with a probability of $T(1 - T)^2$, which yields

$$N_{C+2H} = T(1 - T)N_g + T(1 - T)^2 N_i + T(1 - T)^2 N_m \quad (4)$$

As mentioned earlier, some H and H_2 fragments with high

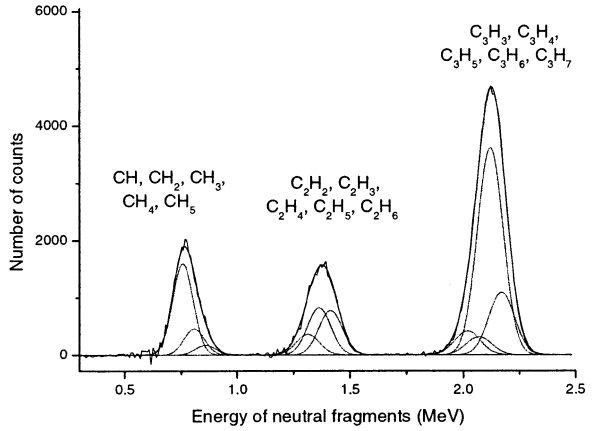

Figure 2. Number of counts vs energy of the neutral fragments detected with the grid in front of the detector. The thin lines are Gaussian fits of the data corresponding to the different neutral fragments. For details see text.

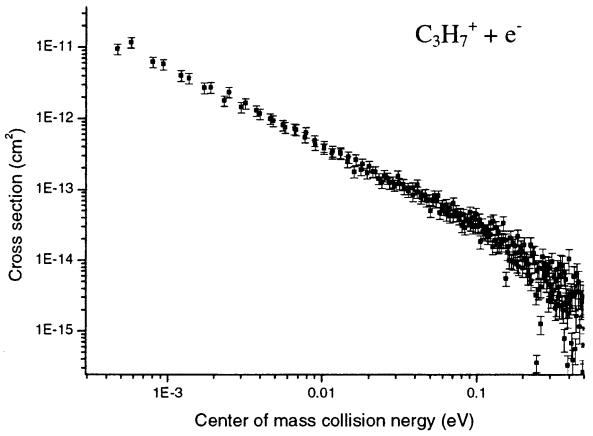

Figure 3. Total cross sections for the dissociative recombination of $C_3H_7^+$ as a function of center of mass kinetic energy.

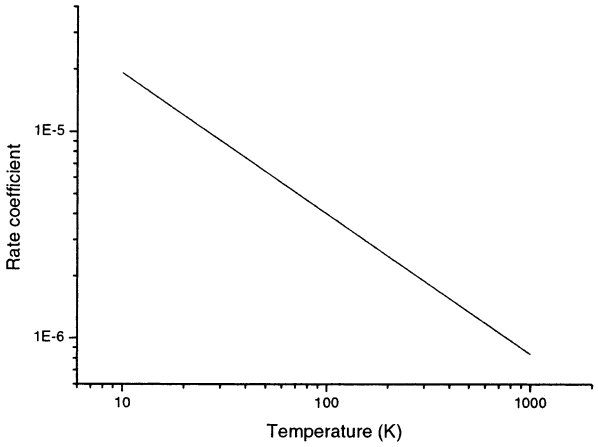

Figure 4. Rate coefficient for the recombination of $C_3H_7^+$ as a function of kinetic temperature.

kinetic energy (greater than 3.2 eV in the present experiment) may not be detected. This means that fragments from these channels may contribute to the peak at a mass $m-m_H$ instead of m, where m is the total mass of the products from a dissociative event and m_H is the mass of the H or H_2 fragment. This has to be taken into account in the equation system. Because the amount of lost particles is unknown, a factor for the loss in each channel was introduced as $L_{H,a}$, $L_{H2,b}$, etc. For example, the contribution from channel a to N_{3C+7H} will be

$$T^2(1 - L_{H,a})N_a \tag{5}$$

The elements subtracted from this peak are added to N_{3C+6H}, for which the contribution becomes

$$T(1 - T)N_a + T^2L_{H,a}N_a \tag{6}$$

The branching fraction for each channel is then given by normalization to the total number of dissociations, i.e.

$$n_i = \frac{N_i}{\sum_i N_i}$$

$$i = a, ..., m \tag{7}$$

The loss of hydrogen from channel a was varied between 10% and 60% in the analysis of the peaks. The discrepancy in branching fractions resulting from this variation is included in the error of the fractions.

Results and Discussion

The measured cross sections are shown in Figure 3 as a function of the center-of-mass collision energy. The statistical uncertainties in the cross section are shown as error bars. The systematical uncertainty is about 15%, based on the error in ion beam current, the length of the electron cooler, the circumference of the storage ring, and the electron density. The cross sections are very large, being greater than 10^{-11} cm^2 at energies below 4 meV. This corresponds to a capture radius of over 200 Å. The cross sections decrease substantially at higher energies with no apparent resonance. There is little scatter in the data in the lowest energy regime; however, at higher energies, where the cross section has dropped by orders of magnitude, the scatter increases significantly due to the signal being only slightly larger than the background value. The cross section data shown in Figure 3 illustrate the relatively large dynamic range of the experiment. On the log−log plot, the data are linear over much of the range. Fitting data with the least amount of scatter (energies from 0.001 to 0.1 eV) yields an energy dependence of $E^{-1.10\pm0.01}$, which is only slightly higher than the E^{-1} dependence predicted by the direct capture mechanism.[24] However, the difference in exponent is statistically significant.

Integrating the energy dependent cross section, $\sigma(E)$, gives the thermal rate coefficient α (in cm^{3}s^{-1}) as a function of the electron temperature T_e:

$$\alpha(T_e) = \frac{8\pi m_e}{(2\pi m_e kT_e)^{3/2}}\int_0^\infty E\sigma(E)e^{-E/kT_e}\,dE \tag{8}$$

Evaluating the integral in eq 8 yields $\alpha(T_e) = (1.9 \times 10^{-6}\pm0.35 \times 10^{-6})\,(T_e/300)^{-0.68\pm0.01}$. The uncertainty is at 1σ level and is based on determinations of the rate while varying the cross sections within its error bars. The rate constant is shown as a function of kinetic temperature in Figure 4. Previously, a value of 8.3×10^{-7} cm^3 s^{-1} was reported for the 300 K rate coefficient based on a flowing afterglow experiment.[25] Throughout the hydrocarbon ion studies in ref 25, the rate coefficient for recombination of O_2^+ was measured as a reference point and was found to be between 1.95×10^{-7} and 2.2×10^{-7} cm^3 s^{-1}. Because that agrees well with the results obtained at CRYRING a few years ago (2.2×10^{-7} cm^3 s^{-1} [26]), the factor of 2 disagreement between the experiments for $C_3H_7^+$ is unexpected.

TABLE 1: Product Branching Ratios for the Reaction $C_3H_7^+ + e^-$[a]

products	label	branching ratio
$C_3H_6 + H$	a	0.42 (0.10)
$C_3H_5 + H_2$	b	0.12 (0.08)
$C_3H_5 + H + H$	c	
$C_3H_4 + H_2 + H$	d	0.09 (0.05)
$C_2H_4 + CH_3$	h	0.04 (0.02)
$C_2H_4 + CH_2 + H$	i	
$C_2H_3 + CH_4$	k	0.19 (0.05)[b]
$C_2H_3 + CH_3 + H$	l	
$C_2H_2 + CH_4 + H$	n	0.11 (0.02)
$C_2H_2 + CH_3 + H_2$	o	
$C_3H_3 + H_2 + H_2$	e	<0.05
$C_2H_6 + CH$	f	
$C_2H_5 + CH_2$	g	
$C_2H_4 + CH + H_2$	j	
$C_2H_3 + CH_2 + H_2$	m	
$C_2H + CH_4 + H_2$	p	

[a] The errors are given at a 1σ level. [b] To form CH_4 rearrangement is necessary, and therefore, channel *l* is more likely than channel *k*; see text.

However, no error is given for the afterglow result, which makes it difficult to assess whether the results overlap at a 3σ level.

The large number of neutral channels potentially available in the dissociative recombination of $C_3H_7^+$, together with the difficulty of adequately resolving features in the recorded pulse height vs energy spectra, makes it impossible to obtain a complete set of branching ratios for all product channels. Given this limitation, we must combine some related two and three body dissociation channels in the analysis. As shown in Table 1, this generally means CH_n products are considered together with the closely related $CH_{n-1} + H$ channel.

The most abundant product channel in the recombination of $C_3H_7^+$ with electrons is loss of a single hydrogen atom, having a branching ratio of 0.42. The measurement does not address which hydrogen is released upon recombination; however, loss of a terminal hydrogen atom suggests a stable alkene (C_3H_6) can form with no additional rearrangement of the remaining hydrogen atoms. If a substantial percentage of the 5.9 eV reaction exothermicity resides as internal energy in the C_3H_6 product, further fragmentation would be expected. Indeed, channels that release multiple hydrogen atoms account for at least another 20% of the overall reactivity. Specifically, channels *b* and *c*, which produce two H atoms or an H_2 molecule, respectively, have a combined branching ratio of 0.11, whereas channel *d*, which produces both a hydrogen atom and a hydrogen molecule, occurs with a branching ratio of 0.09. The possibility of a channel forming two H_2 molecules is grouped into a collection of channels occurring with less than 5% probability. Although the error given in Table 1 are at a 1σ level, the dominance of the combined hydrogen loss channels is statistically significant at a 3σ level.

Although the H-loss channels dominate, the carbon−carbon bond is broken in 34−39% of the recombination reactions, which is considerably more than the 4−18% found for $C_2H_n^+$ systems.[12,13] Unpublished results from Mitchell et al. indicate that an even larger amount, roughly half, of the recombination products from a mixture of $C_4H_9^+$ isomers result from dissociation of carbon−carbon bonds.[27] Exothermicity alone is not the sole driving force because carbon−carbon bond dissociation channels are highly exothermic for C_2, C_3, and C_4 systems. The most abundant C−C bond fission channel for $C_3H_7^+$ involves the formation of a C_2H_3 radical and either CH_4 or $CH_3 + H$. The former requires a concerted decomposition, whereas the latter requires that a terminal CH_3 group is cleaved, followed by loss of H from the remaining radical (or vice versa). The channel corresponding to cleavage of a lone C−C bond accounts for a maximum of 4% of the total reactivity. However, this channel is sufficiently exothermic that subsequent H loss from the remaining C_2 moiety is highly likely. This would lead to the products in channel *l*, which is relatively abundant if the related channel *k* is small. Given the rearrangement necessary to form channel *k*, this seems likely.

Channels *n* and *o* both require substantial rearrangement, leaving a core C_2H_2 molecule and either $CH_4 + H$ or $CH_3 + H_2$. Nevertheless, the combined branching ratio for these channels is 0.11, presumably owing to the stability of the acetylene product. (The C_2H_2 product must be acetylene because the isomerization of vinylidene occurs in about one picosecond.[28]) The remaining channels (*e*, *f*, *g*, *j*, *m*, *p*) comprise at most 5% of the reactivity. These channels require multiple bond dissociations followed by one or two H atoms being transferred. Although these channels are exothermic, in some cases by over 3 eV, they do not play a significant role in the recombination reaction.

In summary, the recombination of $C_3H_7^+$ with electrons has proven to be quite complex. The system can produce 16 separate reaction channels, all of which are highly exothermic. A large number have been observed to occur, although several channels needed to be grouped together because of resolution problems. Hydrogen only loss channels account for more than 60% of the reactivity with the loss of a single H atom being the most probable channel. Breaking one of the C−C bonds accounts for more than a third of the total reactivity, which is considerably higher than what has been found for smaller C_2 hydrocarbon cations. The cross sections for dissociative recombination are very large and decrease as $E^{-1.1}$. At present, this appears to be the largest hydrocarbon cation for which relatively complete branching ratios can be derived since species containing more carbon atoms will have an even larger number of available product channels, and the energy/mass resolution will decrease for a lower energy primary ion beam.

The present results show a much richer chemistry for the recombination of electrons with hydrocarbon cations than has been assumed in the plasma enhanced combustion models. In addition to producing, on average, a larger number of radical species than assumed, the termination step in the ion cycle also appears to contribute to further cracking of the larger fuel fragments. When incorporated into the models, both of these effects should show an even larger enhancement of combustion efficiency resulting from plasma reactions.

Acknowledgment. We thank the staff members of the Manne Siegbahn Laboratory for valuable assistance during the experiment. This work was supported by the Swedish Research Council, the EOARD under Contract F61775-01-WE035, and the IHP Program of the EC under Contract HPRN-CT-2000-00142. J.S. was supported in part by the State Committee for Scientific Research (Poland) under contract 146/E-346/SPUB-M/5. A.A.V. and S.T.A. acknowledge financial support provided by the United States Air Force Office of Scientific Research under Project No. 2303EP4.

References and Notes

(1) Williams, S.; Bench, P. M.; Midey, A. J.; Arnold, S. T.; Viggiano, A. A.; Morris, R. A.; Maurice, L. Q.; Carter, C. D. *JANNAF 25th Airbreathing Propulsion Meeting*, Monteray, CA 2000; p 205.

(2) Viggiano, A. A.; Willians, S. *Adv. Gas-Phase Ion Chem.* **2001**, *4*, 85−136.
(3) Bardsley, J. N.; Biondi, M. A. *Adv. At. Mol. Phys.* **1970**, *6*, 1.
(4) Mitchell, J. B. A. *Phys. Rep.* **1990**, *186*, 215.
(5) Mitchell, J. B. A.; Rebrion-Rowe, C. *Int. Rev. Phys. Chem.* **1997**, *16*, 201.
(6) Larsson, M. *Annu. Rev. Phys. Chem.* **1997**, *48*, *151*.
(7) Larsson, M. In *Advanced Series in Physical Chemistry, Vol. 10B: Photoionization and Photodetachment*; Ng, C.-Y., Ed.; World Scientific: Singapore, 2000; Part 2, p 693.
(8) Larsson, M. In *Advances in Gas-Phase Ion Chemistry*; Adams, N. G., Babcock, L. M., Eds.; JAI Press: New York, 2001; Vol. 4, p 179.
(9) Larsson, M.; Thomas, R. *Phys. Chem. Chem. Phys.* **2001**, *3*, 4471.
(10) Andersen, L.; Heber, O.; Kella, D.; Pedersen, H. B.; Vejby-Christensen, L.; Zajtman, D. *Phys. Rev. Lett.* **1996**, *77*, 4891.
(11) Datz, S.; Sundström, G.; Biedermann, Ch.; Broström, L.; Danared, H.; Mannervik, S.; Mowat, J. R.; Larsson, M. *Phys. Rev. Lett.* **1995**, *74*, 896.
(12) Derkatch, A. M.; Al-Khalili, A.; Vikor, L.; Neau, A.; Shi, W.; Danared, H.; af Ugglas, M.; Larsson, M. *J. Phys. B* **1999**, *32*, 3391.
(13) Kalhori, S.; Viggiano, A. A.; Arnold, S. T.; Rosén, S.; Semaniak, J.; Derkatch, A. M.; af Ugglas, M.; Larsson, M. *Astron. Astrophys.* **2002**, *391*, 1159.
(14) Strömholm, C.; Semaniak, J.; Rosén, S.; Danared, H.; Datz, S.; van der Zande, W. J.; Larsson, M. *Phys. Rev. A* **1996**, *54*, 3086.
(15) Simonsson, A. *Nucl. Instr. Methods Phys. Res. A* **1989**, *284*, 264.
(16) Koch, W.; Liu, B.; Schleyer, P. v. R. *J. Am. Chem. Soc.* **1989**, *111*, 3479.
(17) Lias, S. G.; Rebbert, R. E.; Ausloos, P. *J. Am. Chem. Soc.* **1970**, *92*, 6430.
(18) Dymerski, P. P.; Prinstein, R. M.; Bente, P. F., III.; McLafferty, F. W. *J. Am. Chem. Soc.* **1976**, *98*, 6834−6836.
(19) Attina, M.; Cacace, F.; Giacomello, P. *J. Am. Chem. Soc.* **1980**, *102*, 4768−4772.
(20) Williams, S.; Knighton, W. B.; Midey, A. J.; Viggiano, A. A.; Irle, S.; Morokuma, K. *J. Phys. Chem.* Submitted.
(21) Danared, H. *Phys. Scripta* **1995**, *T59*, 121.
(22) Danared, H.; Källberg, A.; Liljeby, L.; et al. In *Proc. Sixth European Particle Accelerator Conference*; Myers, S., Liljeby, L., Petit-Jean-Genaz, Ch., Poole, J., Rensfelt, K.-G., Eds.; Institute of Physics: London, 1998; p 1031.
(23) Neau, A., Ph.D. Thesis, Stockholm University, Sweden, 2002.
(24) Bardsley, J. N. *J. Phys. B* **1968**, *1*, 365.
(25) Lehfaoui, L.; Rebrion-Rowe, C.; Laubé, S.; Mitchell, J. B. A.; Rowe, B. R. *J. Chem. Phys.* **1997**, *106*, 5406.
(26) Peverall, R.; Rosén, S.; Peterson, J. R.; Larsson, M.; Al-Khalili, A.; Vikor, L.; Semaniak, J.; Bobbenkamp, R.; Le Padellec, A.; Maurellis, A. N.; van der Zande, W. J. *Chem. Phys.* **2001**, *114*, 6679.
(27) Mitchell, J. B. A.; Rebrion-Rowe, C.; Le Garrec, J. L.; Angelova, G.; Andersen, L. H.; Bluhme, H.; Moller, S. P.; Siersen, K. in preparation.
(28) Carrington, T., Jr.; Hubbard, L. M.; Schaefer, H. F., III.; Miller, W. H. *J. Chem. Phys.* **1984**, *80*, 4347.